CMOS CAMERA-BASED OBSERVATION AND CHARACTERIZATION OF MULTIPACTING DURING CAVITY CONDITIONING

L. Bauer*[1,2], A. Ateş[1], J. Kaiser[1,2], P. Müller[1], U. Ratzinger[1,2], H. Hähnel[1,2]
[1]Institute of Applied Physics, Goethe University Frankfurt, Frankfurt am Main, Germany
[2]Helmholtz Forschungsakademie Hessen für FAIR (HFHF), Frankfurt am Main, Germany

Abstract

Raspberry Pi cameras (single board CMOS cameras) have already been successfully implemented for ion beam characterization at IAP Frankfurt and are now also being used to investigate multipacting during cavity conditioning. Multipacting appears caused by resonant secondary electron emission. For the standalone RF conditioning of the FRANZ (Frankfurt Neutron Source) RFQ (Radio-Frequency Quadrupole) and the IH-DTL (Interdigital H-mode Drift-Tube-Linac), these cameras were installed both inside and outside the vacuum to detect multipacting and other cavity glowing effects. The occurrence of multipacting at specific power levels within the cavities can be confirmed by simulations. In addition, the observed multipacting is characterized through spectrometer measurements.

INTRODUCTION

At the Institute of Applied Physics (IAP) in Frankfurt, CMOS cameras combined with single-board computers (Raspberry Pi) have been successfully used for ion beam diagnostics [1, 2] and are now applied for the visualization and analysis of multipacting and other optical effects within cavities. This contribution reports results from the standalone conditioning of the RFQ and the IH-DTL at power levels up to 70 kW and 5 kW, respectively. Both cavities are components of the FRANZ project [3] and are finally operated as one cavity .Based on the optical observations of the positions within the cavities where multipacting appears, calculations based on CST simulations have been performed to confirm the appearance of multipacting at specific power levels [4].In addition to the optical analysis of multipacting, further characterization was done by performing mass spectrometer measurements at the RFQ during conditioning.

CAVITY CONDITIONING AND MULTIPACTING

Conditioning describes the gradual increase in RF power coupled into a cavity to achieve stable high-power operation. The FRANZ cavities are conditioned at low RF levels with duty cycles of 90 % to 100 % to ensure an optimal preparation for operation, whereas duty cycles of 1 % to 2 % are applied during beam operation.

A primary challenge addressed during this phase is multipacting, a resonant electron multiplication phenomenon. This process is initiated by free electrons gaining kinetic energy from the oscillating RF field and colliding with e.g. the cavity walls [5].If these remain in phase with the RF field, an exponential electron avalanche can develop within a few RF cycles, potentially degrading cavity performance [6].To identify multipacting regions computationally, a plane-parallel surface approximation is used, with multipacting predicted on paths with a length of x_0 in voltage ranges

$$V_{\min} = \frac{m_e \omega^2 x_0^2}{2e\sqrt{4 + (2n+1)^2 \pi^2}}. \quad (1)$$

and

$$V_{\max} = \frac{m_e \omega^2 x_0^2}{2e}. \quad (2)$$

where n is an integer describing the order of the multipacting. The frequency f is set to 175 MHz for the given cavities. V_{max} represents the limit beyond which multipacting is not longer possible [7].

MEASUREMENT POSITIONS

Single-board CMOS cameras (Raspberry Pi module V3 and module V3 wide) were used to monitor optical emissions caused by multipacting and other optical phenomena in the RFQ and the IH-DTL during conditioning. The analog gain, white balance (AWB), and focal length were fixed after calibration. Additional to the cameras a mass spectrometer and an optical spectrometer were installed at the RFQ. In Fig. 1 the positions of the installed cameras (also the corresponding field of view (FoV)), mass spectrometer and optical spectrometer at the RFQ to characterize multipacting are shown. Camera RFQ-2 provides a direct view of a stem and a small section of the electrodes, while camera RFQ-1 offers a broader view including a stem, its neighboring stems, a larger section of the electrodes, and the RFQ exit. To improve the image quality of camera RFQ-1, which is affected by radiation-induced pixel artifacts, a 3D-printed PETG-Tungsten shielding is currently under investigation [8].
Figure 2 illustrates the position of both outside the cavity installed cameras and their FoVs. Due to its small FoV camera IH-1 will not be further considered here. Camera IH-2 offers a direct view through a grid on the drifttubes and on the tuner nearby the exit of the cavity.

MULTIPACTING CHARACTERIZATION DURING CONDITIONING

Optical multipacting effects were reproducibly observed at the specific positions in defined power level ranges within the FoVs. Figure 3 shows multipacting events in the RFQ acquired with camera RFQ-1 (left) and camera RFQ-2

* l.bauer@physik.uni-frankfurt.de

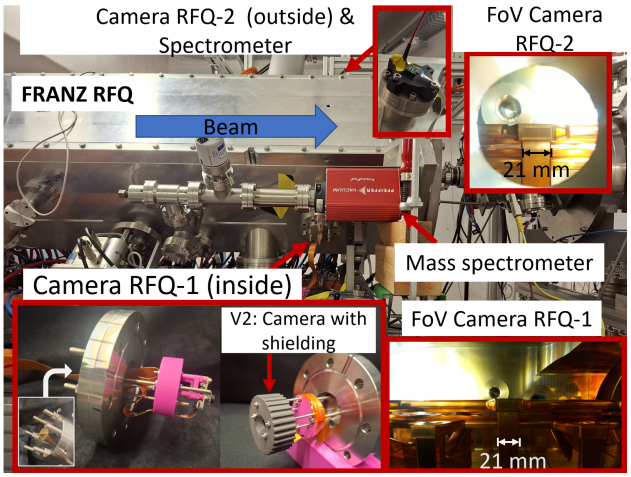

Figure 1: Positions of the installed cameras, the mass spectrometer, and the optical spectrometer at the RFQ. The lower-left corner of the image shows Version 1 of the installed camera in the RFQ, alongside Version 2, which contains a 3D-printed PETG-Tungsten shielding.

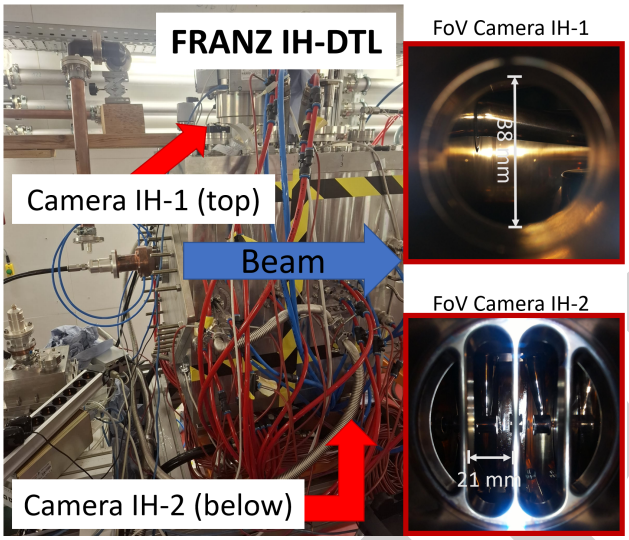

Figure 2: Positions of the cameras installed on the IH-DTL.

(right) at a forward power of 50 W and 100 W, respectively. The residual gas fluorescence is located behind the stems of the electrodes.

In Fig. 4 (left) multipacting appearing in the IH-DTL at a forward power of 110 W and also a reflection on the tuner, reproducible appearing from approximately 50 W on for a camera exposure time of 60 s is shown. This reflection is caused by a glowing point. Multipacting is predominantly observed on the outer surfaces of the drift tubes, especially in the regions facing the gaps, see Fig.4 (right). By analyzing the pixel intensity values (brightness) in the acquired images, a correlation between image intensity and multipacting signatures, such an increase in reflected power and cavity pressure can be found, see Fig.5. During conditioning, mass spectra in the m/z range of 0 to 50 were acquired. During conditioning, additional mass peaks appear in some spec-

Figure 3: Left: Multipacting appearing at a forward power of 50 W acquired with the camera installed inside (camera RFQ-1) the RFQ. Right: Multipacting appearing at forward power of 100 W acquired with the camera installed outside (camera RFQ-2) the RFQ on the viewport. Both images are acquired with an exposure time of 60 s.

Figure 4: Left: Multipacting appearing at a forward power of 110 W in the IH cavity. Right: Multipacting is observed on the outer surfaces of the drift tubes facing the gaps. The reflection on the tuner is also visible as a reddish spot on the left side. Both images are acquired with an exposure time of 60 s.

tra (Fig. 6, bottom), which correlate with the presence of multipacting. At higher power levels above the multipacting threshold, these additional peaks coincide with observed luminous effects.

CALCULATION OF MULTIPACTING ZONES

CST Eigenmode simulations were used to determine field values and voltages along selected paths. Based on the observed multipacting locations, representative straight electron paths with a length x_0 (see Eq(1)) within the FoVs of the cameras were considered. In Fig. 7 a comparison is shown between the theoretically predicted power levels for which multipacting is expected based on the resonance condition, Eq(1) and the experimentally set power levels at which multipacting is observed within the cameras' FoVs. Overall, a good agreement can be demonstrated for both cavities between the calculated and experimentally observed power levels for the occurrence of multipacting. The resulting discrepancies between the calculated and the experimentally observed multipacting ranges may arise from insufficient brightness in the images.

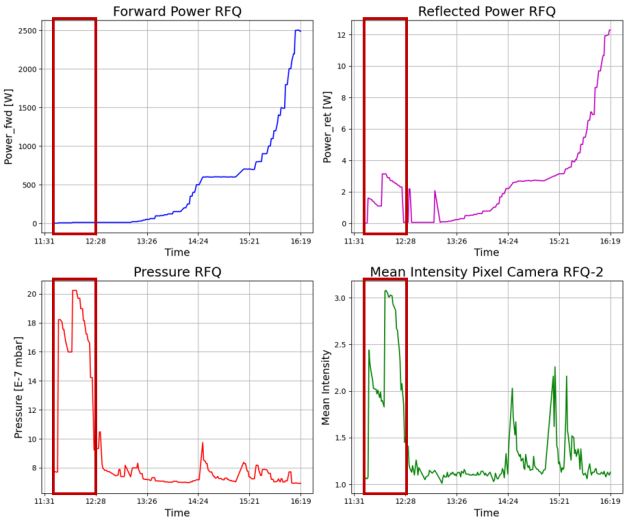

Figure 5: Logged data of forward power (blue curve), reflected power (purple curve), cavity pressure (red curve), and image brightness (green curve) during RFQ conditioning from 0 W to 25 kW. The correlation between the cavity parameters and the optical appearance (image brightness) of multipacting is visible within the red-highlighted rectangles.

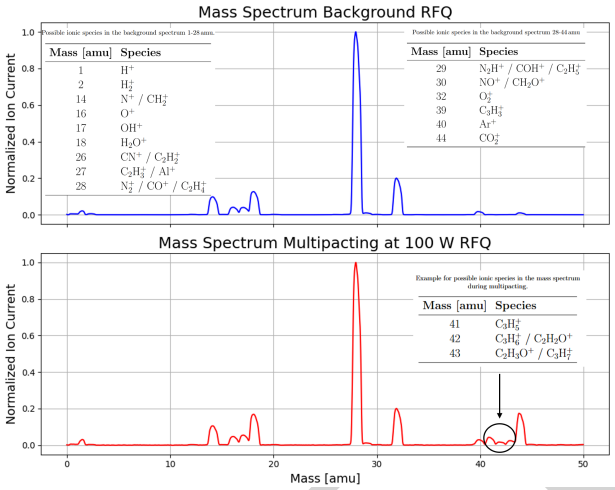

Figure 6: Top: Background mass spectrum of the RFQ acquired in the absence of any observable optical effects. The table lists possible ion species. Bottom: Example mass spectrum acquired during multipacting in the RFQ (also confirmed by optical observations). In addition to the background, several additional mass peaks are present. Possible ion species are listed in the table.

CONCLUSION AND OUTLOOK

CMOS cameras enable the detection of optical multipacting, which occurs reproducibly within specific power ranges and can be confirmed by image brightness alongside the cavity data such as e.g. reflected power. Calculations based on the resonance condition show good agreement with experimentally observed power levels for multipacting. The results indicate, that the camera based observation of the positions of multipacting can be used for further calculations. Mass spectra correlate multipacting and optical effects with characteristic peaks, while optical spectra remain inconclusive due to low intensity. Ongoing and future work includes a radiation shielding for improving the image quality and advanced simulations (using e.g. CST particle solver). An enhanced diagnostics such as mass sepctra in a wider range (0-100) and an optical spectrometer upgraded with a collimator should be applied. The integration of an image intensifier with significantly shorter exposure times is proposed to enable quasi-time-resolved observation of individual discharges. A characterization of multipacting appearing in the coupled RFQ and IH-DTL cavities, with particular attention to differences in behavior compared to standalone conditioning is planned.

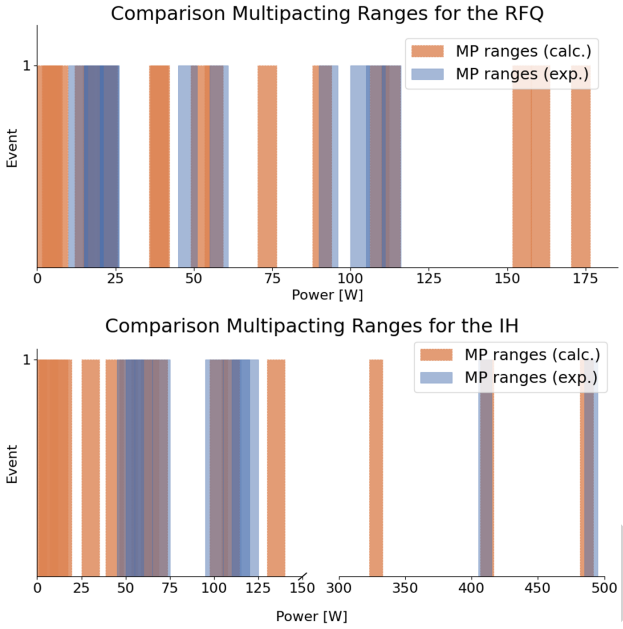

Figure 7: Comparison between the multipacting zones calculated using the resonance condition (orange) and those experimentally observed as optical effects in the acquired images during standalone conditioning (blue) of the RFQ (top) and the IH-DTL (bottom). Calculated power ranges for a few exemplary straight paths within the cameras' FoVs.

ACKNOWLEDGMENTS

We would like to thank Prusa Polymers for providing the PETG-Tungsten Filament for this experiment.

REFERENCES

[1] A. Ateş *et al.*, "Raspberry Pi cameras as beam induced fluorescence monitors for low and high energy beams", in *Proc. IPAC'23*, Venice, Italy, May 2023, pp. 4692–4695. doi:10.18429/JACoW-IPAC2023-THPL100

[2] A. Ateş *et al.*, "Raspberry Pi cameras for beam diagnostics at the Frankfurt Neutron Source", in *Proc. IPAC'25*, Taipei, Taiwan, Jun. 2025, pp. 3141–3143. doi:10.18429/JACoW-IPAC2025-THPS087

[3] H. Hähnel *et al.*, "Upgrade and commissioning of the 60 keV low energy beam transport line for the Frankfurt Neutron

Source FRANZ", in *Proc. LINAC'22*, Liverpool, UK, Aug. 2022, pp. 352–355. doi:10.18429/JACoW-LINAC2022-TUPOJO08

[4] Dassault Systèmes, *CST Studio Suite: User Manual*, Version 2024, Darmstadt, Germany, 2024.

[5] V. D. Shemelin and S. A. Belomestnykh, *Multipactor in Accelerating Cavities*. Cham, Switzerland: Springer, 2020. doi:10.1007/978-3-030-48198-8

[6] R. Prakash *et al.*, "Multipacting studies in elliptic SRF cavities", *Nucl. Instrum. Methods Phys. Res. A*, vol. 867, pp. 128–138, 2017. doi:10.1016/j.nima.2017.06.003

[7] T. P. Wangler, *RF Linear Accelerators*, 2nd ed. Weinheim, Germany: Wiley-VCH, 2008. doi:10.1002/9783527623426

[8] Prusa Research, *Prusament PETG Tungsten 75: Material Datasheet*, accessed Apr. 2026. https://www.prusa3d.com/de/produkt/prusament-petg-tungsten-75-1kg-nfc/